ELSEVIER

Materials Science and Engineering A298 (2001) 63–72

MATERIALS SCIENCE & ENGINEERING A

www.elsevier.com/locate/msea

Transformation-mismatch plasticity of NiAl/ZrO_2 composites — experiments and continuum modeling

Peter Zwigl [a,1], David C. Dunand [b,*]

[a] *Department of Materials Science and Engineering, Massachusetts Institute of Technology, Cambridge, MA 02139, USA*
[b] *Department of Materials Science and Engineering, Northwestern University, Evanston, IL 60208, USA*

Received 2 May 2000; received in revised form 12 July 2000

Abstract

NiAl composites containing 10 and 20 vol.% unstabilized zirconia particles were thermally cycled around the polymorphic phase transformation range of zirconia while being subjected to an external uniaxial tensile stress. The strain rate of the composite during thermal cycling is significantly higher than the isothermal creep rate of either composite or unreinforced matrix at the same average temperature. An established model for transformation-mismatch plasticity of an allotropic, creeping metal has been adapted to describe the results. To the best of our knowledge, this is the first demonstration of transformation-mismatch plasticity in a composite induced through transformation of the minority-phase reinforcement. © 2001 Elsevier Science B.V. All rights reserved.

Keywords: Phase transformations; Superplasticity; Creep; NiAl; ZrO_2; Metal matrix composites

1. Introduction

NiAl stands out among potential replacements for nickel-based superalloys because of its low density, large stoichiometric range, high melting point, good thermal conductivity, low raw materials cost and outstanding oxidation resistance [1,2]. However, NiAl is brittle at low temperature and creeps rapidly at elevated temperature. Both problems can be addressed by adding a strong ceramic second phase to NiAl, which increases toughness by interfacial debonding and improves creep resistance by load transfer. Shaping of ceramic particulate-reinforced NiAl composites is however very difficult. Casting is limited by the high melting point of NiAl, its reactivity with most ceramics and the phase segregation occurring due to the density difference between the solid reinforcement and the liquid matrix. Powder-metallurgy techniques usually require a final machining step, which is difficult because of the brittleness of the composite and the hardness of the reinforcement.

Superplastic forming is a possible solution to the problem of shaping particulate-reinforced NiAl composites. However, microstructural superplasticity requires very fine grains (typically less than 10 μm) which are difficult to achieve and maintain in NiAl. Transformation superplasticity, on the other hand, occurs independently of the grain size, as it relies on internal mismatch stresses produced during cyclical polymorphic phase transformations. Transformation superplasticity has been reported in allotropic metals and polymorphic alloys, as reviewed in, e.g. Refs. [3,4] and recently in the Ti_3Al-based super-α_2 intermetallic subjected to thermal cycles about the α_2–β phase transformation [5]. While NiAl does not exhibit any phase transformation, a suitable polymorphic ceramic reinforcement within a NiAl matrix can produce internal mismatch stresses in the composite, inducing transformation-mismatch plasticity, or upon multiple cycling, transformation superplasticity. Unstabilized zirconia is an attractive choice, because it is chemically inert with NiAl, its strength and stiffness are higher than NiAl and its monoclinic (m) to tetragonal (t) phase transformation occurs within a temperature range where NiAl

* Corresponding author. Tel.: +1-847-4915370; fax: +1-847-4676573.
E-mail address: dunand@northwestern.edu (D.C. Dunand).
[1] Present address: Intel Corp., 1900 Prairie City Road, Folson, CA 95630, USA.

PII: S0921-5093(00)01343-5

deforms rapidly by creep and is associated with a large volume change. All conditions for transformation-mismatch plasticity are thus met: large internal stresses can be created by ZrO_2 transformation within a NiAl matrix, which can deform rapidly by creep under an externally-applied biasing stress.

Transformation superplasticity in metal matrix composites was recently demonstrated in the Ti/TiC [6,7], Ti–6Al–4V/TiC [8,9], Ti–6Al–4V/TiB [10] and Fe/TiC [11] systems, for which the matrix is polymorphic while the particulate reinforcement is inert. The present paper examines, for the first time, the complementary case, i.e. a composite where the minority, discontinuous phase (ZrO_2 particles) undergoes a phase transformation while the majority, continuous phase (NiAl matrix) is inert. To the best of our knowledge, this is also the first demonstration of transformation-mismatch plasticity in an intermetallic composite system.

2. Materials and experimental procedures

Two types of unstabilized zirconia particles were used. First, particles produced by Tosoh (Tokyo, Japan) were annealed for 48 h at a temperature of 1500°C and sieved between −230 mesh and +270 mesh. The powders were fed through a spinning tube held at an angle of 30° to separate spherical particles from blocky particles, resulting in hollow ZrO_2 spheres with a mean diameter of 60 μm. Second, zirconia particles manufactured by Ferro (Cleveland, OH) were annealed at 1550°C for 96 h and separated mechanically into two fractions with average diameters of 60 and 180 μm, respectively. NiAl powders from Cerac (Milwaukee, WI) with a particle size between 44 and 100 μm and a purity of 99.5% were mixed for 12 h in a V-blender with 10 and 20 vol.% ZrO_2 powders. The mixtures were cold-pressed into low-carbon steel cans (lined with a 100-μm thick molybdenum foil to prevent contamination), degassed under vacuum at elevated temperature, and compacted by hot-isostatic-pressing for 6 h at a pressure of 103 MPa and a temperature of 1163°C. In addition to an unreinforced NiAl control billet, four NiAl/ZrO_2 billets were produced, consisting of three composites with 10 vol.% ZrO_2 having fine-, medium- and large-size particles (10, 60, 180 μm, respectively) and one composite with 20 vol.% ZrO_2 large particles (180 μm).

Table 1
Transformation temperatures on heating $T_{m/t}$ and cooling $T_{t/m}$ of annealed zirconia particulates and a NiAl/10ZrO_2-60μm composite

Material	$T_{m/t}$ (°C)	$T_{t/m}$ (°C)	Method
Particulates (Tosoh)	1193	1043	Calorimetry
Particulates (Ferro)	1093	952	Calorimetry
Composite (Ferro)	1076	894	Dilatometry

Table 2
Temperature cycle characteristics and effective creep parameters (Eqs. (2) and (3))

Cycle	T_l (°C)	T_u (°C)	ν (h^{-1})	K_{eff} (s^{-1})	E_{eff} (GPa)
A	700	1200	7.5	3.85×10^8	151
B	850	1250	10	1.20×10^9	147
C	750	1150	15	8.70×10^7	151

The transformation temperatures of the zirconia particles were determined by differential thermal analysis (Perkin Elmer-Series 7) under heating and cooling rates of 10 K min^{-1} in air with alumina as reference material (Table 1). To determine the transformation temperatures of the zirconia within the composite, dilatometry (Netzsch-ES 402) was performed on diamond-ground, parallelepiped samples (2.3 mm × 3 mm × 12 mm) under the same conditions.

Diamond-ground, flat tensile specimens (gauge length: 20 mm, width: 6 mm, thickness: 2.3 mm) were tested in a custom-designed creep apparatus described in more detail in Ref. [12], which allows for the application of small tensile stresses with simultaneous rapid temperature cycling in an argon atmosphere. Three types of temperature cycles with various amplitude and frequency were used (Table 2). Before thermal cycling, the samples were crept isothermally at the upper cycle temperature until a steady-state strain rate was reached. The deformation was measured by an inductive linear displacement transducer placed at the cold end of the load-train. Under cycling conditions, the deformation measured by the transducer thus included the thermal dilatation of pullrods, grips and sample, and did not represent the sample plastic strain. However, the strain measured under isothermal conditions or over an entire temperature cycle was only due to the sample plastic deformation. The plastic strain increment per cycle, $\Delta\varepsilon_{tot}$, was calculated as the average of four to six steady-state cycles. After cycling, isothermal creep was again measured at the upper cycling temperature. This procedure was repeated until failure of the sample.

Metallographic samples were polished with 6 and 3 μm diamond paste and with a colloidal silica suspension, followed by etching with Kallings reagent (5% $CuCl_2 \cdot xH_2O$ in a 1:1 mixture of HCl and H_2O). Density measurements using the Archimedes principle were performed on as-processed samples and on segments of the gauge section after deformation.

3. Results

Fig. 1a–d show micrographs of the materials after host-isostatic pressing, illustrating that the grain size of

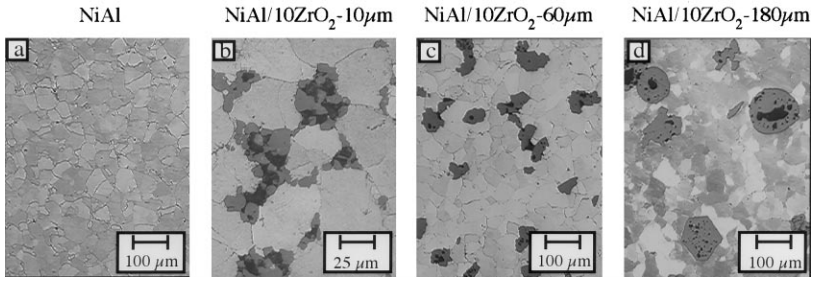

Fig. 1. Micrographs of NiAl and NiAl/10ZrO_2 after hot-isostatic pressing.

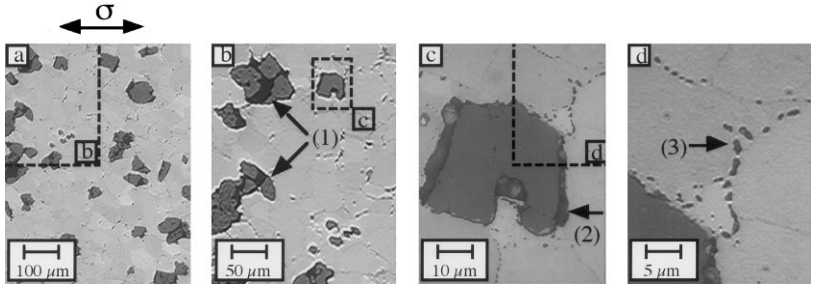

Fig. 2. Micrograph of NiAl/20ZrO_2-180 μm after creep deformation (a) with magnified details (b), (c) and (d).

the NiAl matrix is ~ 40 μm. After compaction, the hollow, spherical 60 μm ZrO_2 Tosoh particles were crushed to an average size of 10 μm, while the Ferro powder size (60 and 180 μm) remained unchanged. The microstructure of NiAl/20ZrO_2-180 μm after creep deformation is shown at increasing magnification in Fig. 2a–d.

Table 1 shows that both ZrO_2 powders exhibit a hysteresis of ~ 145 K between the m/t (heating) and t/m (cooling) transformation, and that the transformation temperatures are ~ 100 K higher for the Tosoh powders than for the Ferro powders. Dilatometric measurements of the NiAl/10ZrO_2-60 μm composite showed the m/t transformation on heating at $T_{m/t} =$ 1076°C with a contraction of $|\Delta L/L|_h = 0.13\%$ and the t/m transformation on cooling at $T_{t/m} = 894$°C with an expansion of $|\Delta L/L|_c = 0.10\%$.

The steady-state isothermal strain-rate $\dot{\varepsilon}$ for unreinforced NiAl and the NiAl/ZrO_2 composites is plotted in Fig. 3, as a function of stress σ at various temperatures T according to a power-law equation:

$$\dot{\varepsilon} = \frac{A}{T}\exp\left(-\frac{Q}{RT}\right)\left(\frac{\sigma}{E}\right)^n \quad (1)$$

where E (GPa) $= 199.8 - 0.040T$ (K) [1] is the elastic modulus of NiAl, Q the creep activation energy, n the stress exponent, R the gas constant and A the pre-exponential factor. The reinforcement was in the tetragonal phase, except for the composite with 10 μm particles tested at 1175°C. Best-fit of the creep data gives $A = 1.6 \times 10^{25}$ K s^{-1}, $n = 3.9$ and $Q = 318$ kJ mol^{-1} for unreinforced NiAl, in good agreement with values reported by Vandervoort et al. [13] ($n = 3.8$–4.4 and $Q = 300$ kJ mol^{-1}) for cast NiAl deformed in compression for similar stresses ($\sigma = 6.5$–43 MPa) and temperatures ($T = 1100$–1250°C). The best-fit of the composite creep data yields $n = 3.5$ and $Q = 330$ kJ mol^{-1} with pre-exponential factors $A = 2.7 \times 10^{24}$ and 1.3×10^{24} K s^{-1} for fine (10 μm) and coarse (60 and 180 μm) particulates, respectively. As seen in Fig. 3, the presence of particulates has little effect on the isothermal creep rate of NiAl, and there is no difference between the composites with 10 and 20 vol.% ZrO_2.

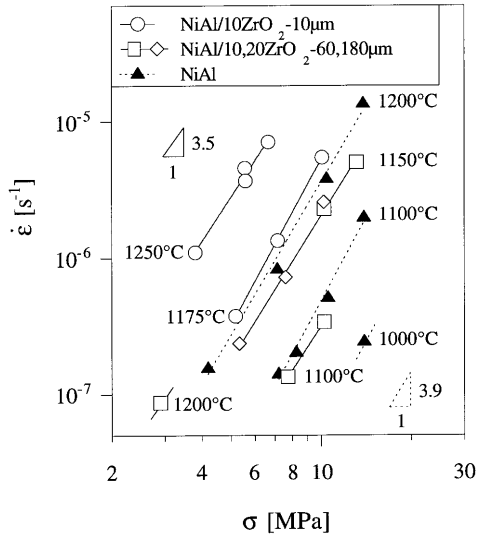

Fig. 3. Isothermal steady-state creep rate as a function of applied stress for NiAl and NiAl/ZrO_2 composites with different particle size and volume fraction.

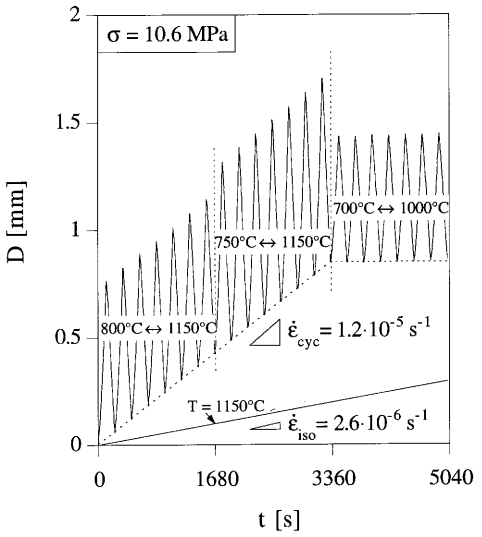

Fig. 4. Total deformation of the load train as a function of time at $\sigma = 10.6$ MPa for a NiAl/20ZrO_2-180 μm composite during thermal cycling (with three different cycling characteristics at $v = 15$ h^{-1}) and during isothermal creep. Slopes correspond to sample average strain rates.

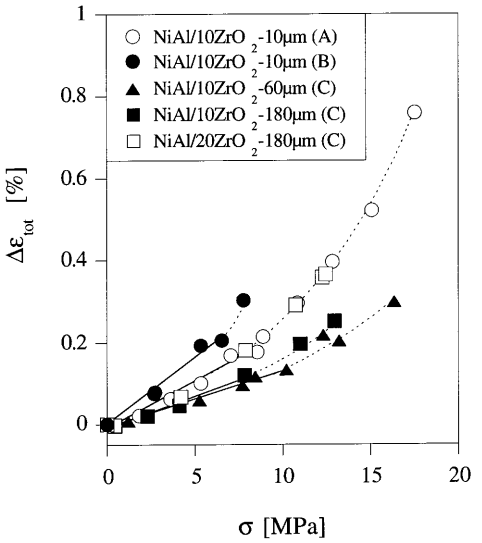

Fig. 5. Total strain increment per cycle as a function of the applied stress for NiAl/ZrO_2 composites, with different particle volume fractions, particle sizes, and temperature cycles (A–C, as given in Table 2).

Fig. 4 shows the experimentally measured displacement of the load train as a function of time at $\sigma = 10.6$ MPa for a NiAl/20ZrO_2-180 μm composite for three types of thermal cycles and during isothermal creep. The three cycling segments were concatenated on Fig. 4 and transients associated with the temperature change are not shown. In the isothermal case, steady-state deformation occurs at 1150°C at a rate $\dot{\varepsilon} = 2.6 \times 10^{-6}$ s^{-1}. The cycles show the reversible thermal expansion and contraction of the load train and the irreversible permanent plastic strain increments, $\Delta\varepsilon_{tot} = 0.29\%$, accumulated after each cycle, corresponding to an average strain rate $\dot{\varepsilon} = v\Delta\varepsilon_{tot} = 1.2 \times 10^{-5}$ s^{-1} for the cycling frequency $v = 15$ h^{-1}. The strain increment is constant for the first two cycle ranges (800–1150°C and 750–1150°C) which encompass both transformation temperatures (894 and 1076°C), but it drops to zero for the third cycle range (700–1000°C) which does not cross the m/t transformation temperature.

In Fig. 5, the strain increment per cycle is plotted as a function of the applied stress for all specimans tested. For all composites, the strain increment is initially proportional to the applied stress, but increases non-linearly for higher stress values. Considering composites with Ferro particles subjected to 750–1150°C cycles, data for the two composites with 10 vol.% ZrO_2 overlap, while larger strain increments are found for the composite containing 20 vol.% particles. Similarly, larger strain increments are found for composites with 10 vol.% Tosoh particles cycled to a higher upper temperature ($T_u = 1200$ and 1250°C).

Experiments were conducted until failure, which occurred after a strain of 14–30% had been accumulated within the gage section, as measured on the fractured samples (Table 3). Fracture occurred in the gage or the sample heads, which also showed significant plastic deformation. While the head deformation may have contributed significantly to the total cyclic strain, this systematic error can be assumed to affect all samples roughly equally, because the same sample geometry was used for all specimens.

4. Discussion

4.1. Materials

The measured density of the unreinforced NiAl (5.92 g cm^{-3}, Table 3) is close to the values reported in the literature (5.90 [1] and 5.85 g cm^{-3} [2]), indicating full densification after processing. Porosity levels between 0.2 and 0.9% were measured for the NiAl–10% ZrO_2 composites and 2.3% for the NiAl–20% ZrO_2 composites (Table 3), and can be explained by residual porosity in some of the largest zirconia particles (Fig. 1c,d). Also, the crushing of the hollow, large Tosoh zirconia particle lead to somewhat porous clusters of particles in the composites with 10 μm particles (Fig. 1b). Composites with larger, uncrushed particles displayed a good particle distribution (Fig. 1c,d). Finally, the 40 μm grain size of the NiAl matrix visible in Fig. 1b–d is well above the typical upper limit of 10 μm for microstructural plasticity by grain-boundary sliding to occur. The absence of microstructural superplasticity is confirmed by the isothermal creep results showing a stress exponent $n = 3.5$–3.9 for all materials (Fig. 3).

Table 3
Measured density after processing ρ_{HIP}, sample porosity, particle volume fraction f and strain to fracture ε_{frac}

Composition	ρ_{HIP} (g cm^{-3})	Porosity (%)		f (%)	ε_{frac} (%)
		as HIP	Fractured		
NiAl	5.92	0	0	0	6
NiAl/10ZrO_2-10 μm	5.84	1.0[a]	3.8	9.7	30
NiAl/10ZrO_2-60 μm	5.87	0.5[b]	1.5	9.9	23
NiAl/10ZrO_2-180 μm	5.83	1.2[b]	2.1	9.8	14
NiAl/20ZrO_2-180 μm	5.73	2.6[b]	4.0	19.3	16

[a] Porosity in matrix.
[b] Porosity in particles.

The composites after creep deformation showed porosity at particle clusters (arrow (1) in Fig. 2b) and at particle–matrix interfaces oriented perpendicular to the applied stress (arrow (2) in Fig. 2c). Also visible in Fig. 2d (arrow (3)), are fine micron-size precipitates at grain boundaries, possibly alumina particles resulting from the partial reduction of ZrO_2 by aluminum in the matrix (both NiAl and ZrO_2 can be non-stoichiometric).

The hysteresis in transformation temperature upon heating and cooling of the loose powders reported in Table 1 is a well-known feature of the diffusionless, martensitic transformation in zirconia [14,15]. The magnitude of undercooling depends on the crystallite size and purity of the zirconia powder [16]. The zirconia particles within the composite were found to transform at lower temperatures than for unconstrained powders (Table 1), as qualitatively expected from the constraining effect of the matrix during the phase transformation. Table 1 shows that this decrease upon cooling (58 K for the t/m transformation) is larger than upon heating (17 K for the m/t transformation). This can be justified by the fact that the polymorphic transformation temperature is lower on cooling, so that the matrix is stronger and can exert a larger constraint on the transforming particles. The higher matrix constraint also explains the smaller composite length change during the t/m transformation on cooling (0.10%) than during the m/t transformation on heating (0.13%).

4.2. Thermal cycling of $NiAl/ZrO_2$ composites

An average strain rate $\dot{\varepsilon}_{cyc} = \nu\Delta\varepsilon$ can be determined for the thermal cycling experiments as shown in Fig. 4. To compare these average thermal-cycling strain rates with isothermal strain rates, the dimensionless, temperature-averaged plot of Fig. 6 can be utilized, using temperature-averaged constants for the cycled specimens given as:

$$K_{eff} = \frac{A}{\Delta t}\int_0^{\Delta t} \frac{\exp(-Q/RT(t))}{T(t)}\,dt \quad (2)$$

$$E_{eff} = \frac{1}{\Delta t}\int_0^{\Delta t} E(T(t))\,dt \quad (3)$$

and listed in Table 2 for each cycle.

In Fig. 6, both the large increase in deformation rate upon cycling and the low cycling stress exponent close to unity (also listed in Table 4) are strong indications of a material deforming by transformation-mismatch plasticity. Tensile elongations in excess of 100%, necessary to demonstrate transformation superplasticity upon repeated cycling, were however not achieved due to premature fracture in the specimen head. Nevertheless, Table 3 shows that substantial elongations were reached in the cycled composites ($\varepsilon_{fract} = 14$–30%), significantly larger than for unreinforced NiAl deformed under isothermal conditions ($\varepsilon_{fract} = 6\%$), so it is likely that superplastic elongation can be attained in the future by decreasing the stress concentration at the loading pin. Table 3 also indicates that cavitation is only modest (porosity is increased by 1–3% at fracture). As expected, cavities form preferentially at the

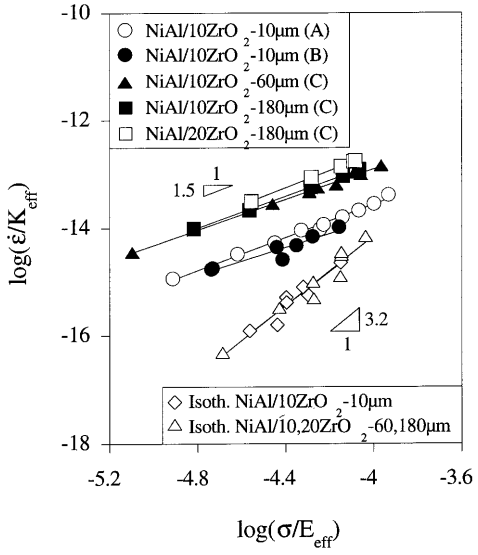

Fig. 6. Temperature-compensated plot of average creep rate vs. stress for $NiAl/ZrO_2$ composites deformed isothermally and upon thermal cycling with various temperature cycles (A–C, as given in Table 2).

Table 4
Slopes ($d(\Delta\varepsilon_{tot})/d\sigma$, $d(\Delta\varepsilon)/d\sigma$) from the linear part of Fig. 5 before and after creep correction, effective internal stress $\sigma_{0,eff}$ calculated from Eq. (6) and effective stress exponent n_{eff} from Fig. 6

Composite	Cycle	$d(\Delta\varepsilon_{tot})/d\sigma$ (GPa^{-1})	$d(\Delta\varepsilon)/d\sigma$ (GPa^{-1})	$\sigma_{0,eff}$ (MPa)	n_{eff}
NiAl/10ZrO_2-10 μm	A	0.23	0.19	15.4	1.5
NiAl/10ZrO_2-10 μm	B	0.34	0.29	10.1	1.3
NiAl/10ZrO_2-60 μm	C	0.14	0.13	22.9	1.4
NiAl/10ZrO_2-180 μm	C	0.16	0.15	19.7	1.5
NiAl/20ZrO_2-180 μm	C	0.23	0.23	22.6	1.6

matrix–particle interface oriented perpendicular to the applied stress, as shown in Fig. 2c.

The load–train displacement recorded at the end of each half-cycle on heating ΔD_h and on cooling ΔD_c (Fig. 4) can be written as:

$$\Delta D_{h,c} = \pm \Delta D_{cte} + \Delta D_{creep} + \Delta D_{tp} \quad (4)$$

where ΔD_{cte} is the magnitude of the load–train displacement due to the thermal expansion (or contraction) on heating (or cooling), ΔD_{creep} is the displacement due to sample creep at temperatures where the sample is not undergoing a transformation and ΔD_{tp} is the displacement caused by transformation-mismatch plasticity. For small specimen length changes, ΔD_{cte} is fully reversible over a whole thermal cycle, whereas ΔD_{creep} and ΔD_{tp} result in irreversible plastic strains at the end of each half-cycle. At low stresses where ΔD_{creep} is negligible as compared with ΔD_{tp} and where ΔD_{tp} is proportional to the applied stress, Eq. (4) can be approximated by:

$$\Delta D_{h,c} \approx \pm \Delta D_{cte} + \frac{d(\Delta\varepsilon_{h,c})}{d\sigma} L\sigma \quad (5)$$

where $\Delta\varepsilon_{h,c}$ is the strain increment per transformation and L is the sample gauge length. Thus, the slope of a plot of ΔD_h (or ΔD_c) versus $L\sigma$ gives the stress-normalized strain increment $d(\Delta\varepsilon_{h,c})/d\sigma$ for transformation on heating and cooling, without creep contribution.

Fig. 7 shows such plots for NiAl with 10 vol.% ZrO_2. This figure indicates that all the deformation occurs in the heating part of the cycle ($d(\Delta\varepsilon_h)/d\sigma = 0.15\ GPa^{-1}$) during and following the m/t transformation at 1076°C, with no deformation on the cooling half of the cycle ($d(\Delta\varepsilon_c)/d\sigma = 0\ GPa^{-1}$). This is in contrast to pure metals such as zirconium, where the above analysis showed that transformation-mismatch strains are equal upon transformations on heating and cooling [12]. We believe that the reason for this difference is that the transformation temperatures for NiAl/ZrO_2, unlike zirconium, are very different on heating and cooling. Thus, while the mismatch strains produced during the m/t transformation on heating at 1076°C can be accommodated by rapid creep of the NiAl matrix, the relatively low temperature of the t/m transformation on cooling at 894°C prevents rapid accommodation by creep of NiAl.

A first possibility is that mismatch strains due to the t/m transformation are accommodated elastically by the NiAl matrix. If no relaxation were to occur upon subsequent heating up to the m/t transformation temperature, these elastic stresses would be cancelled by that transformation at 1076°C, with no net transformation plasticity at the end of the cycle. However, as transformation plasticity is clearly occurring in a repeatable manner upon multiple cycling, this scenario requires that stored elastic strains produced by the t/m transformation on cooling are released during the heating period by matrix creep before the m/t transformation temperature is reached. Then, the transformation-mismatch strain developed during the heating half-cycle ($d(\Delta\varepsilon_h)/d\sigma = 0.15\ GPa^{-1}$) consists of two contributions: a first contribution (accumulated in the temperature interval 894–1076°C) due to mismatch produced at 894°C during the t/m transformation in the previous cooling half-cycle, and a second contribution (accumulated between 1076°C and T_u) due to mismatch produced at 1076°C by the m/t transformation. Finally, we note that the dilatometry experiment, performed at

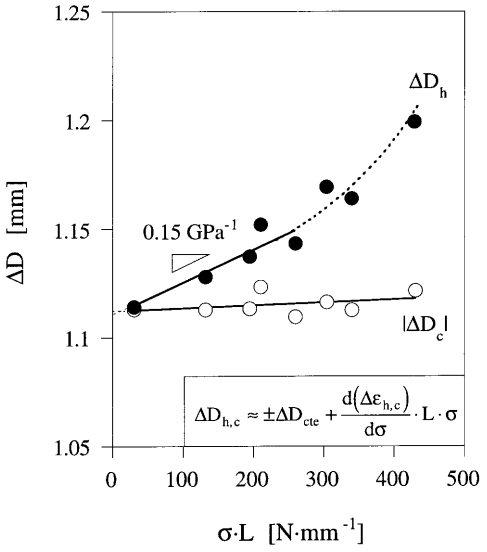

Fig. 7. Deformation difference of the heating- and cooling part of the temperature cycle as a function of the product of the applied stress with the instantaneous sample length for NiAl/10ZrO_2-60 μm with temperature cycle (C).

a much lower cooling rate (slower by a factor 45), showed that internal strains could be relaxed during the t/m transformation on cooling ($|\Delta L/L|_c = 0.10\%$). This lends credence to our hypothesis that mismatch strains are indeed produced at the m/t transformation during rapid cooling, but that their relaxation by matrix creep does not occur in the short time spent cooling the sample to T_l (43 s for cycle C).

An alternate explanation for the lack of measurable transformation plasticity on cooling (Fig. 7) assumes that mismatch produced during the t/m transformation is accommodated by time-independent yield. Matrix plasticity is then expected to occur around the particles, resulting in a shell of plastically-deformed matrix of radius c, given for the case of thermal expansion mismatch as [17]:

$$c = r\left[\frac{\Delta\alpha\Delta T E}{(1-\nu)\sigma_y}\right]^{1/3} \tag{6}$$

where ν is the Poisson's ratio, σ_y is the yield stress, $\Delta\alpha$ is the thermal expansion difference between matrix and particles and ΔT is the thermal excursion. Numerical calculations presented in a companion paper [18] indicate that the maximum Mises stress in the matrix at the particle interface is on the order of 800 MPa, much higher than the yield stress of polycrystalline NiAl at 894°C ($\sim$100 MPa [1,2]). However, the actual yield stress of the matrix near the particles may be significantly larger for three reasons: (i) the yield stress of NiAl at those temperatures increases with increasing strain rate [1,2] and the transformation (and thus the local strain rate in the matrix near the particles) is very rapid; (ii) addition of as little as 0.1 at.% Zr to NiAl increases the yield stress by a factor of two to three [1,2], and some dissolution of the ZrO_2 in contact with NiAl during processing and testing is very likely; (iii) NiAl strain-hardens at these temperatures [1,2] and the matrix region around the particles is expected have a very high dislocation density. Taking a credible value of the effective local yield stress of 400 MPa and replacing the thermal mismatch term $\Delta\alpha\Delta T$ in Eq. (6) with the polymorphic mismatch $|\Delta V/V|/3$ (where $\Delta V/V$ is the polymorphic volume change between the two zirconia phases), Eq. (6) predicts a plastic zone with a diameter twice that of the particle. Assuming 10 vol.% equisized particles packed according to a FCC lattice, more than a quarter of the matrix would not be plastically deformed, and the plastic zones surrounding particles would barely overlap. As seen in Fig. 1b–d, particles size and distribution are however far from ideal, and a plastic zone extending one radius beyond the particle will not lead to a macroscopically connected plastic region in the matrix. A equation based on similar assumptions by Pickard and Derby [19] for the case of thermal-expansion mismatch also predicts no onset of generalized flow in the composite. Then, transformation mismatch on cooling is accommodated by local, time-independent yield around the matrix, which cannot be biased by the external stress since the plastically-deformed matrix is not continuous through the composite. There is thus no macroscopic strain increment on cooling. On subsequent heating, however, mismatch produced by the m/t transformation is accommodated by creep, so that the total transformation plasticity increment at the end of the cycle consists of only the heating contribution.

4.3. Modeling of transformation mismatch plasticity in $NiAl/ZrO_2$

Greenwood and Johnson [20] derived an analytical expression for a pure metal based on continuum mechanics linking the transformation plastic strain increment $\Delta\varepsilon$ caused by a phase transformation to the applied stress σ:

$$\Delta\varepsilon = \frac{2}{3}\left|\frac{\Delta V}{V}\right|\frac{\sigma}{\sigma_0}\frac{5n}{(4n+1)} \tag{7}$$

where $|\Delta V/V|$ is the volume mismatch between the two allotropic phases, and δ_0 and n are the average internal stress and isothermal creep stress exponent, respectively, for the weaker allotropic phase accommodating the internal mismatch. Eq. (7) was developed for transformations at high homologous temperatures where accommodation of the allotropic mismatch is by creep. In the present case, the homologous temperature of NiAl at the m/t transformation of ZrO_2 is $T/T_m = 0.71$ at which power-law creep is indeed rapid (Fig. 3).

Eq. (7) is only valid at low stresses ($\sigma \ll \sigma_0$). As shown by Refs. [5,12,21], a solution valid at all stresses can be expressed as:

$$\overline{\psi} = \overline{(\eta-\gamma)\left(1+\frac{9}{4}\eta^2-\frac{9}{2}\eta\gamma\right)^{\frac{(1-n)}{2n}}} \tag{8}$$

where the bar notation indicates an average over a spherical volume element and where the following dimensionless parameters are used: $\eta = \Delta\varepsilon/(\Delta V/V)$, $\psi = \sigma_{zz}/\sigma_0$, and $\gamma = (\Delta V/V)_{zz}/(\Delta V/V)$, with $(\Delta V/V)_{zz}$ and σ'_{zz} as the zz-components of the mismatch tensor and deviatoric stress tensor. The left-hand side of Eq. (8) is given by $\bar{\psi} = (2/3)(\sigma/\sigma_0) := (2/3)\delta$, while integration of the non-linear right-hand side of Eq. (8) is in general only possible by numerical methods (see Refs. [5,12,21]). Eq. (7) can be expressed in dimensionless form as:

$$\eta = \frac{2}{3}\frac{5n}{(4n+1)}\delta \tag{9}$$

Eqs. (7) and (8) were developed for the case where the entirety of the sample undergoes a phase transformation (e.g. for single-phase materials), unlike NiAl/ZrO_2 where only the reinforcement is polymorphic.

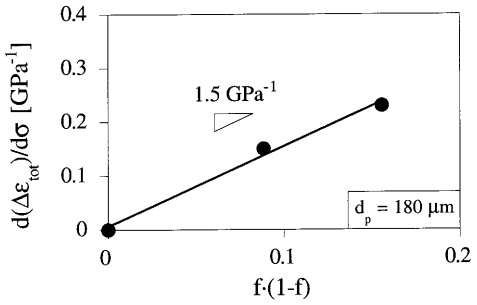

Fig. 8. Transformation-plasticity slope (in Fig. 5) as a function of the volume–fraction parameter $f(1-f)$ for composites with 10 and 20 vol.% ZrO_2.

This situation is similar to the case of thermally-cycled Al–SiC composites, where the internal strains are produced by the mismatch in coefficient of thermal expansion (CTE) between the two phases. For Al–SiC composites, Pickard and Derby [19] defined an effective volume mismatch, $(\Delta V/V)_{\text{eff}}$:

$$\left|\frac{\Delta V}{V}\right|_{\text{eff}} = f(1-f)(3|\Delta\alpha\Delta T|) \tag{10}$$

where f is the volume fraction of the reinforcement, and the last term in brackets is the thermal mismatch. These authors then found a good match with Eq. (7) for composites with various volume fractions and thermal excursions. We take here the same approach but add the contribution $|\Delta V/V|$ from the volume change upon polymorphic transformation (which has the same sign as the thermal mismatch):

$$\left|\frac{\Delta V}{V}\right|_{\text{eff}} = f(1-f)\left(\left|\frac{\Delta V}{V}\right| + 3|\Delta\alpha\Delta T|\right) \tag{11}$$

We now compare the magnitude of the two sources of internal mismatch in Eq. (11) produced by thermal expansion and polymorphic transformation, respectively. Based on the previous observation that mismatch relaxation may not occur in the strong NiAl matrix at the lower range of the temperature cycle, we assume that the thermal expansion mismatch between ~ 950°C and T_l is stored elastically on cooling and subsequently canceled on heating. Similarly, we assume that the thermal excursion between 1076°C and T_u is too rapid and too narrow to produce mismatch plasticity. Then, with an effective thermal excursion $\Delta T =$ 1076–950°C and with literature CTE values at 1076°C for NiAl ($\alpha = 17.4 \times 10^{-6}$ K^{-1} [24]) and for ZrO_2 ($\alpha = 12.0 \times 10^{-6}$ K^{-1} [25]), the CTE mismatch volume strain is $3|\Delta\alpha\Delta T| = 0.20\%$. This value is significantly smaller than the effective polymorphic mismatch ($|\Delta V/V| = 4.3\%$) so that CTE mismatch can be safely neglected in the following.

The validity of using Eq. (11) in Eq. (7) can be verified by plotting the slope $\Delta\varepsilon_{\text{tot}}/\sigma$ as a function of the volume fraction parameter $f(1-f)$. Fig. 8 indeed shows that these two parameters are proportional for NiAl with 10 and 20 vol.% large ZrO_2 particulates. A second verification of Eq. (11) is to consider the measured dilatometric value of the polymorphic contraction $\Delta L/L = 0.13\%$ which should be equal to $|\Delta V/V|_{\text{eff}}/3$ with $\Delta T = 0$. The calculated volume change of the zirconia is then $|\Delta V/V| = 4.3\%$, somewhat smaller than literature values for $|\Delta V/V| = 7.5\%$ [22,23]. This discrepancy can be explained by the porosity within, and at the interface of, the ZrO_2 particles (Fig. 1b–d): by providing space for the particle to freely expand and contract, porosity reduces the mismatch with the matrix during the transformation.

Another prediction of Eq. (7) is that particle size does not affect the strain increment per cycle. This is confirmed in Fig. 5 by the overlap of data for 10 vol.% composites with Ferro particles of two different sizes (60 and 180 μm). However, composites with 10 μm Tosoh particles show much higher $\Delta\varepsilon_{\text{tot}}/\sigma$ slope. One likely reason is that the thermal cycles for these composites extended to higher temperature, so that more creep was accumulated outside the phase transformation. This creep contribution was determined by integrating Eq. (1) over the temperature cycle. Then, the transformation plastic strain increment $\Delta\varepsilon$ was calculated by subtracting the creep strain contribution from the experimental values of $\Delta\varepsilon_{\text{tot}}$. Table 4 lists the corrected slopes $\Delta\varepsilon/\sigma$ which are however still different between composites with 10 vol.% particles subjected to different cycles. An explanation for the discrepancy is that the transformation temperature of the Tosoh zirconia particles is ~ 100°C higher than for the Ferro particles. The weaker NiAl matrix can then accommodate the transformation mismatch more readily, resulting in a higher strain increment per cycle. Finally, for composites with Tosoh particles, the lower $\Delta\varepsilon/\sigma$ slope for cycles with an upper temperature of 1200°C (Table 4) may be explained by the proximity of the transformation temperature (1193°C, Table 1): the real temperature of the composite may have been lower by a few degrees, so that transformation of the particle was incomplete and the strain increment was subsequently lower than for the composite cycled up to 1250°C, well above the transformation temperature.

Fig. 9 shows a comparison of our experimental data with the prediction of Eqs. (8) and (9) with $n = 3.5$ and using $|\Delta V/V| = 4.3\%$ and $\Delta T = 0$ in Eq. (11). The transformation plastic strain increment $\Delta\varepsilon$ was found by subtracting from the experimental values of $\Delta\varepsilon_{\text{tot}}$ the creep strain accumulated during the cycle outside the phase transformation. Furthermore, the effective internal stresses $\sigma_{0,\text{eff}}$ (listed in Table 4) were found by fitting to Eq. (7) the linear slope of plots of $\Delta\varepsilon$ versus σ near the origin using:

$$\sigma_{0,\text{eff}} = \frac{\left|\frac{\Delta V}{V}\right|_{\text{eff}}}{\frac{2}{3}\frac{5n}{(4n+1)}\frac{\mathrm{d}\Delta\varepsilon}{\mathrm{d}\sigma}} \quad (12)$$

Thus, while Eqs. (8) and (9) are strictly valid for a single transformation during a half temperature cycle, we use here the total strain accumulated during a full cycle (from which the creep contribution was subtracted) as well as the average internal stress for both transformations.

Despite the many adaptations made to adapt the complicated case of $NiAl/ZrO_2$ to that of a pure allotropic metal given by Eqs. (8) and (9) (i.e. effective volume mismatch, strain increments and internal stresses averaged over a full cycle), all experimental data in Fig. 9 collapse on a single curve in good agreement with theory. Fig. 9 also shows that the linear Eq. (9) coincides with the non-linear Eq. (8) for stresses up to $\sigma/\sigma_0 = 0.55$. With the exception of the two highest stress points (which have the highest uncertainty in the creep correction), data for $\sigma/\sigma_0 > 0.55$ seems to follow the non-linear Eq. (8), as also observed in zirconium [12] and titanium aluminide [5]). The good overlap for all four composites and three cycles also confirms that transformation-mismatch plasticity is independent of ZrO_2 particle size or cycle frequency, as expected from continuum theory. Cycle amplitude does not affect transformation-mismatch plasticity $\Delta\varepsilon$ (Fig. 9) but controls the amount of creep accumulating outside the transformation range, so that the total strain increment $\Delta\varepsilon_{\text{tot}}$ is different for different upper and lower cycling temperatures (Fig. 5).

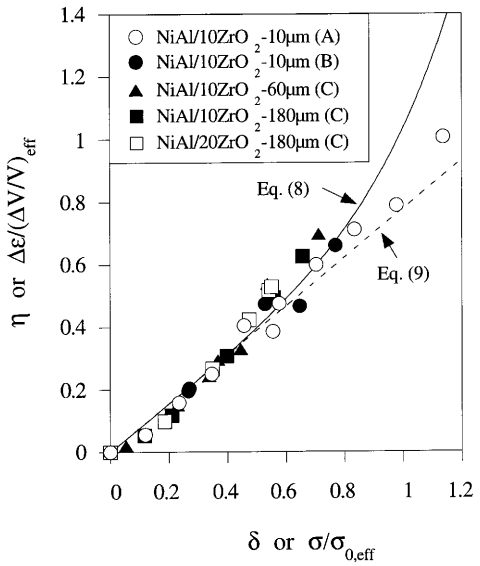

Fig. 9. Transformation-plasticity strain increment (normalized by the effective polymorphic mismatch) as a function of applied stress (normalized by the effective internal stress). Data points for all composites in Fig. 5 and curves according to theory.

5. Conclusions

Composites consisting of a NiAl matrix reinforced with 10 and 20 vol.% zirconia particles 10–180 μm in size were thermally cycled about the polymorphic transformation temperature range of zirconia while being subjected to an uniaxial tensile stress.

The average strain rates under thermal cycling conditions were much higher than those under equivalent isothermal conditions. The linear relationship between strain increment per cycle and applied stress indicates that the composite deforms by transformation-mismatch plasticity. This mechanism results from the biasing by the external stress of internal mismatch stresses produced in the matrix by the transformation of the zirconia particles. To the best of our knowledge, this is the first report of transformation-mismatch plasticity in an intermetallic matrix composite or in any composite system where the reinforcement is polymorphic and the matrix non-transforming.

Because total sample elongation was limited by fracture at the specimen heads, transformation-mismatch superplasticity could not be demonstrated. However, tensile strains as large as 30% were achieved upon multiple cycling of the composites.

Transformation-mismatch plasticity was observed only during the heating half-cycle and not during the cooling half-cycle. We believe this is because mismatch strains produced during the cooling transformation at 894°C are stored elastically in the strong matrix and subsequently relaxed by matrix creep at higher temperature during the following heating half-cycle. The transformation temperature on heating (1076°C) is however high enough for polymorphic mismatch to induce matrix creep which is biased by the applied stress.

Transformation-mismatch plasticity continuum mechanics models, which were originally developed for a single-phase allotropic material undergoing complete transformation without temperature hysteresis, can be adapted to describe the $NiAl/ZrO_2$ results by using an effective transformation mismatch strain taking into account the volume fraction of transforming second phase. As expected, the strain increment per cycle is not affected by the ZrO_2 particle size, the cycling frequency or the upper and lower temperatures of the cycle. These temperatures however determine the amount of strain accumulated during the cycle by isothermal creep outside the transformation range.

Acknowledgements

This study was supported by the US Army Research Office (grant DAAH004-95-1-0629) when both authors were at the Department of Materials Science and Engineering of the Massachusetts Institute of Technology

(MIT). DCD also acknowledges the support of AMAX in the form of a career development chair at MIT.

References

[1] R.D. Noebe, R.R. Bowman, M.V. Nathal, Int. Mater. Rev. 38 (1993) 193.
[2] D.B. Miracle, Acta Metall. Mater. 41 (1993) 649.
[3] T.G. Nieh, J. Wadsworth, O.D. Sherby, Superplasticity in Metals and Ceramics, Cambridge University Press, Cambridge, 1997.
[4] D.C. Dunand, in: T. Chandra, T. Sakai (Eds.), International Conference on Thermomechanical Processing of Steels and Other Materials, TMS, Warrendale, PA, 1997, p. 1821.
[5] C. Schuh, D.C. Dunand, Acta Mater. 46 (1998) 5663.
[6] D.C. Dunand, C.M. Bedell, Acta Mater. 44 (1996) 1063.
[7] C. Schuh, D.C. Dunand, Scripta Mater. 40 (1999) 105.
[8] D.C. Dunand, S. Myojin, Mater. Sci. Eng. 230 (1997) 25.
[9] C. Schuh, W. Zimmer, D.C. Dunand, in: R.S. Mishra, A.K. Mukherjee, K.L. Murty (Eds.), Creep Behavior of Advanced Materials for the 21st Century, TMS, Warrendale, PA, 1999, p. 61.
[10] C. Schuh, D.C. Dunand, Int. J. Plastic (in press).
[11] P. Zwigl, D.C. Dunand, Metall. Mater. Trans. A 29 (1998) 565.
[12] P. Zwigl, D.C. Dunand, Metall. Mater. Trans. A 29 (1998) 2571.
[13] R.R. Vandervoort, A.K. Mukherjee, J.E. Dorn, Trans. ASM 59 (1966) 931.
[14] G.M. Wolten, J. Am. Ceram. Soc. 46 (1963) 418.
[15] P. Orlans, L. Montanaro, J.P. Lecompte, B. Guilhot, A. Negro, in: S. Meriani, C. Palmonari (Eds.), Zirconia'88, Elsevier Applied Science, Barking, UK, 1988, p. 219.
[16] H.S. Maiti, K.V.G.K. Gokhale, E.E. Subbarao, J. Am. Ceram. Soc. 55 (1972) 317.
[17] D.C. Dunand, A. Mortensen, Acta Metall. Mater. 39 (1991) 127.
[18] P. Zwigl, D.C. Dunand, Mater. Sci. Eng. A, submitted.
[19] S.M. Pickard, B. Derby, Acta Metall. Mater. 38 (1990) 2537.
[20] G.W. Greenwood, R.H. Johnson, Proc. Royal Soc. Lond., 1965, p. 403.
[21] W. Mitter, Umwandlungsplastizität und ihre Berücksichtigung bei der Berechnung von Eigenspannungen, Gebr. Bornträger, Berlin, 1987.
[22] M. Rühle, W.M. Kriven, in: H.I. Aaronson, D.E. Laughlin, R.F. Sekerka, C.M. Wayman (Eds.), Solid–Solid Phase Transformations. Met. Soc. of AIME, Carnegie-Mellon University, 1981, p. 1569.
[23] M.B. Bever, Encyclopedia of Materials Science and Engineering, Pergamon Press, Oxford, 1986.
[24] R.W. Clark, J.D. Whittenberger, in: T.A. Hahn (Ed.), Thermal Expansion, vol. 8, Plenum Press, Oxford, 1981, p. 189.
[25] Y.S. Touloukian, R.K. Kirby, R.E. Taylor, T.Y.R. Lee, Thermal Expansion: Nonmetallic Solids, IFI/Plenum, New York, 1975.